Current Applied Science and Technology Vol. 23 No. 6 (November-December 2023)

Research article

Dewetting Behavior of PS-ZnO Thin Film Coated on Ultrathin Au Layer Grown on Si Substrate

Nampueng Pangpaiboon[1]*, Wararak Kotpech[1], Thanaboon Ketkaew[1], Bancha Arthibenyakul[1], Natt Klaewklar[2], Varisara Chanprasopchai[2], Chayatid Sutthi[2], Komsun Lapawae[3] and Kitiphat Sinthiptharakoon[3]

[1]*Department of Industrial Physics and Medical Instrumentation, Faculty of Applied Science, King Mongkut's University of Technology North Bangkok, Bangkok, Thailand*
[2]*Samsen Wittayalai School, Bangkok, Thailand*
[3]*National Nanotechnology Center (NANOTEC), National Science and Technology Development Agency (NSTDA), Phathum Thani, Thailand*

Received: 21 September 2022, Revised: 10 December 2022, Accepted: 14 March 2023

DOI: 10.55003/cast.2023.06.23.005

Keywords

thermal dewetting;
surface energy;
electronic structure;
ultrathin gold film;
polystyrene thin film;
ZnO additive

Abstract

Electronic packaging by coating device component surfaces with polymer thin film is an important step to protect the components from harsh environments. However, along with the device miniaturization to improve its performance, scaling down the coating film can cause a decrease in film durability. Therefore, the thermal stability of pure polystyrene (PS) and zinc oxide-incorporated polystyrene (PS-ZnO) nano-thin films coated on gold (Au) layer with different nano thicknesses on Si substrate were examined to determine the smallest Au thickness at which the polymer films would exhibit optimal stability, and to investigate the effects of the Au component on film resistance to thermal dewetting. With the requirement of having a transparent and conductive Au electrode, the thickness of 20 nm was identified as the optimal value for the Au layer on which both the PS and PS-ZnO films could withstand environment temperatures at 150ºC for up to a few hours while the PS-ZnO film exhibited outstanding thermal stability for over 10 days. Such excellent durability was ascribed to the physio-chemical framework in which the coating film can experience forces from the coated layers which potentially affect the mobility of polymer chains. Considering the increase of Au content and Au film roughness with increasing Au film thickness and realizing the similar surface adhesion forces of these Au layers, several possible influences of the Au material on the stability of PS matrix were discussed. The findings provide an insight into heat-resistant coatings for nano-thin Au layers grown on Si, which may also be of benefit in the design and understanding of relevant electronic protection and functional polymeric coatings.

*Corresponding author: Tel.: (+66) 25552000
E-mail: Nampueng.p@sci.kmutnb.ac.th

1. Introduction

Electronic packaging is a manufacturing step performed to protect electronic device components such as metallic electrodes on semiconductor substrates from harmful environments, e.g., device operation temperatures of higher than 100ºC. Among the various protection methods that rely on either operation protocol or device structure design, the coating of component surfaces with polymer thin film has often been the method of choice due to its low cost, specific weight, and ease of fabrication [1]. However, miniaturizing polymer film to nanoscale thickness severely decreases its thermal stability. Contact imperfection at the polymer/metal interface leads to hole or void formations that can dramatically cause film rapturing at around the glass transition temperature (T_g) of the polymer. This thermal breakdown is known as thermal dewetting [2-7]. The incorporation of nanoparticles into polymer matrix is considered as a potential solution due in part to the physical interaction between the polymer and the embedded nano-additives which helps reduce polymer chain dynamics, and thereby enhancing film stability [8-12]. Various nanoparticles have been discovered to be effective dewetting inhibitors, and examples include silver (Ag) [4], titanium dioxide (TiO_2) [13], and zinc oxide (ZnO) [14-16]. Previously, we also found that an appropriate concentration of ZnO nanoparticles added into polystyrene (PS) nanofilm coated on silicon (Si) substrate efficiently suppressed the dewetting of coating film at environmental temperatures of higher than100ºC [14-16].

Since a coating film can experience forces from the coated surface (e.g., Debye force and van der Waal force) that affect the mobility of polymer chains [17], coating components other than the film should also contribute to the suppression of thermal dewetting. Notably, the effect of surface energy of the coated layer on the dynamics of added nanoparticles was discussed in 2015 by Roy *et al*. [12] who found that nanoparticle concentration could influence nanoparticle location in the polymer film. Additionally, the correlation between the surface energies of coated surface and mixed nanoparticles was also reported to play an important role in the dewetting inhibition mechanism [16]. Although it is still under debate whether the nanoparticles form an interfacial layer between the coated surface and the coating film which improves film stability through the effect of pinning contact line [16, 18], or whether they are distributed throughout the film [15], the influence of the coated surface is non-negligible. Hence, the consideration of device component parameters together with coating film characteristics is useful for packaging design and understanding.

In this work, the thermal stability of PS and PS-ZnO nano-thin films coated on gold (Au) electrode layers of different nanoscale thicknesses deposited on Si substrate is investigated. The objective is to identify the smallest nano-thickness of a Au layer on which the polymeric film exhibits the optimum resistance to thermal dewetting. The selection of Au is not only because Au is an intensively used material as the conducting part in Si-based electronic circuits but also because Au can provide additional electronic-based properties (e.g., sensing) to the polymer film via atomic diffusion. In fact, both factors benefit from the miniaturization of material dimensions [19-21]. ZnO is employed as an additive mainly to improve thermal resistance; however, it also provides the possibility of adding other functions to the coating film such as antibacterial activities [22, 23] and pH sensing [24], properties for which ZnO is well-known. The difference in nanoscale thickness of Au layer was examined based on a physio-chemical framework in which the polymeric coating film could experience forces from the Si substrate [17]. The work was particularly focused on Au thickness of around 10-20 nm that were optically transparent while electrically conductive, thereby allowing the penetration of illuminating light toward the Si base layer [25] and having the potential to be used in light-controlled electronic devices such as transistor-based sensor which might require a transparent gate [26]. Additionally, the Fermi level of Si, which influences its energy-band bending near the surface (i.e., surface potential), was also examined through the variation of Si doping concentration.

In this work, the thermal dewetting of coating films is compared using optical microscopy (OM) and scanning electron microscopy (SEM) data to calculate the percentage of dewetting area. Despite the fact that PS and PS-ZnO films on the thicker Au films exhibit the desired thermal stability, by considering the above-mentioned criteria of Au layer, a Au film of 20 nm thick was identified as the optimal thickness. The PS-ZnO coating film on 20 nm Au has better thermal resistance when compared to the coating film on 10-nm Au film. To understand the causes of this, topographical data in correlation with the surface adhesion forces of the Au films simultaneously acquired using atomic force microscopy (AFM) is analyzed. Together with the surface energies of the coating films obtained from contact angle (CA) analysis, the effect of interfacial electronics and morphology on polymer chain mobility is discussed. The findings provide insights into the heat-resistance coating of nano-thin Au layer on Si using nano-thin PS film which can benefit the design and understanding of electronic packaging and functional polymeric coatings.

2. Materials and Methods

2.1 Materials

Two types of Si wafers, undoped Si (Si1E0) and n-type Si with doping concentration of 1×10^{17} atom/cm^3 (Si1E17), were cut into pieces of 1 cm (width) × 1 cm (length) × 0.5 mm (thickness) in size. The substrates were cleaned using sonication for 10 min, separately, in each of the following solutions in the order as follows: acetone, de-ionized (DI) water, isopropanol, and ethanol. After that, the silicon substrates were dried by blowing with nitrogen gas. The Au target of 99.99% purity with 54 mm (diameter) × 0.1 mm (thickness) (Electron Microscopy Sciences) was installed as the sputtering target for the Au film growth on Si. PS (Alfa Aesar) having molecular weight of 30,000 g/mol (PS30K) was used as the polymer matrix. ZnO nanoparticles, which were to function as additives, and most of which were of sizes larger than 50 nm, were visualized by transmission electron microscopy (TEM) (JEOL JEM-2100Plus) as shown in Figure 1. Toluene (Fisher Chemical) was used as the solvent.

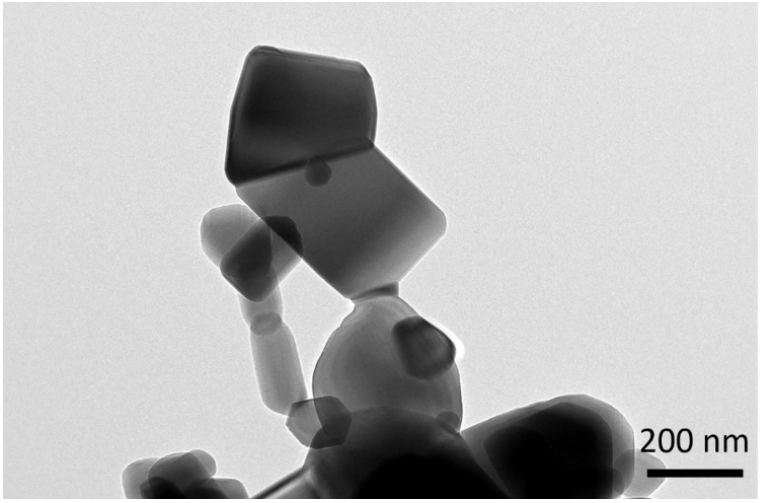


Figure 1. TEM image of ZnO nano-additives (magnification 40,000X)

2.2 Gold layer

For the Au layer fabrication, while physical vapor deposition (PVD) and molecular beam epitaxy (MBE) techniques were also favorable [27], magnetron sputtering was chosen by considering obtainable film quality with strong adhesion to the substrate at relatively low costs [28]. Au nano-thin layers were grown on the Si substrates using the direct-current (DC) sputtering technique under high vacuum (Leica, Mikrosysteme GmbH). The sputtering process was operated at 10^{-2} mbar under 18 sccm of argon gas. The deposition rate was 0.05 nm/s. The sputtering deposition parameters are shown in Table1. The topography images of the Au layers were acquired using AFM (Bruker JPK). Their surface energies were calculated based on contact angle analysis using two types of liquids - DI water and diiodomethane. On the basis of Owens and Wendt's equation as shown in equation (1) [29], surface energy (γ) was evaluated. Subscripts S, L, and V represented solid, liquid, and vapor, respectively. Superscripts d and h represented the polar and non-polar components while θ is the contact angle. The surface energies of water (γ_{water} = 72.7, γ^{d}_{water} = 21.8, and γ^{h}_{water} = 50.9 mJ.m^{-2}) and diiodomethane ($\gamma_{diiodomethane} = \gamma^{d}_{diiodomethane}$ = 50.0 and $\gamma^{h}_{diiodomethane}$ = 0 mJ.m^{-2}) were used for the calculation.

$$\gamma_{LV}(1 + \cos\theta) = 2\left(\sqrt{\gamma^{d}_{SV}\gamma^{d}_{LV}} + \sqrt{\gamma^{h}_{SV}\gamma^{h}_{LV}}\right) \quad (1)$$

Table 1. The values of sputtering deposition parameters

Deposition parameter	Value
Current	30 mA
Deposition rate	0.05 nm/s
Base pressure	10^{-7} mbar
Operating pressure	10^{-2} mbar
Substrate-to-target distance	15-20 cm

2.3 PS and PS-ZnO thin film

PS solution was prepared by mixing PS powder at 0.5 wt.% in toluene solvent. Similarly, the suspension of ZnO nanoparticles was prepared by mixing ZnO nanoparticles 0.5 wt.% in toluene solvent. To produce the PS-ZnO composite solution, the ZnO suspension was dropped into the PS solution at 0.5 wt.% concentration. Ultrasonication was used to homogenize the mixture for 5 min. A 0.2 mL droplet of either PS solution or PS-ZnO solution was deposited on the Au layers on Si before spin-casting (MTI, VTC-100). Notably, the spin-casting technique has been confirmed to provide reproducible production in a short time and at low cost [30]. The spinning rate was 1000 rpm for 10 s. The PS and the PS-ZnO thin films were then dried at room temperature for 24 h before characterization using OM (Olympus, CX31) for morphology checking and CAM for contact angle analysis.

2.4 Dewetting behavior

Annealing a polymer film at a temperature higher than its glass-transition temperature generates dewetting. Hence, the PS and PS-ZnO thin films coated on the Au layers were heated in a vacuum oven (Binder, VD 23) at the temperature of 150°C from 0 to 240 h (10 days), under the pressure of 5 mbar to check their dewetting behavior. Changes in the surface topographies of the PS and the PS-ZnO thin films were observed using an OM and SEM (FEI, Quanta 250). Dewetting areas were analyzed, using at least three SEM images per sample in conjunction with an image analysis

program. Next, the percentage of dewetting area was calculated, as shown in equation (2). A schematic diagram of the experiment is shown in Figure 2.

$$\%\ dewetting\ area\ =\ \frac{dewetting\ area}{total\ area} x100 \qquad (2)$$



Figure 2. Schematic diagram of the experiment

3. Results and Discussion

3.1 Morphology and formation of Au layer on Si substrate

Compared with the topographical image of bare Si surface, Figure 3, which shows the topographical images of Au layers of different thicknesses on Si1E0 and Si1E17, demonstrates that the Si surfaces are fully covered by the Au films. Note that the Au thicknesses were obtained from the thickness values displayed on the sputtering instrument which provided approximately the same magnitudes as measured using SEM and AFM in our previous work [25]. With decreasing thickness, the Au film surface on both Si substrates was revealed to consist of irregular grain shapes which can be viewed as labyrinthine structure [31]. Considering that the morphological characteristics of the coated surface can help stabilize the polymer chains of coating film (e.g., PS film), this disordered surface configuration could increase chain pinning and thereby enhance the resistance of the coating film to thermal dewetting. However, it is noteworthy that the thicker the Au film is, the rougher the Au film surface becomes, regardless of Si doping concentrations. The roughness parameter (R) may be more involved in the dewetting inhibition.

Notably, for each Au thickness, the Au films on Si1E0 exhibit slightly smoother surfaces than the Au films on Si1E17. Moreover, for each thickness of less than 30 nm, smaller Au cluster sizes and shorter inter-distance between the clusters are observed in the cases of Si1E0 compared to the cases of Si1E17. This observation implies that the Au layers on Si1E0 experience less attractive interaction from the Si surface than those Au layers grown on Si1E17 [32]. This suggests the effect of Si substrate potential related to Si Fermi level and thereby Si doping concentration. Despite the Si effect on the formation of Au layers, the consideration of the surface adhesion force of the Au films which shows independence of Au film thickness suggests that the potential influence from Si would not have a significant impact on the surface of these Au films. Moreover, referring to our previous work that showed that the Au film of as thin as 10 nm on the Si substrate is conductive [25], the samples with 10-nm and 20-nm Au thicknesses will be considered onwards. The selection is based on the criteria that the obtained Au layer should be optically transparent while being electrically conductive.

3.2 Morphology and composition of As-cast PS and PS-ZnO thin films

Figure 4 shows the PS and the PS-ZnO film thicknesses coated on those Au layers grown on Si substrates. It is obvious that polymer film thickness increases from ~ 9 nm to ~ 18 nm when the Au layer thickness decreases from 20 nm to 10 nm. Notably, the polymer thickness on 10-nm Au layer is comparable to that on bare Si. Recalling that the interactions from the supports including Si and Au may affect the mobility of polymer chains, the thinner polymeric coating film should possess superior thermal stability to the thicker film. The consideration indicates that the PS films and the PS-ZnO films on 20-nm Au layer should exhibit stronger resistance to thermal dewetting than these films on 10-nm Au layer.

After resting the polymeric coating films at room temperature for 24 h, the films were inspected using the OM technique. Figure 5 shows the OM images of the PS and the PS-ZnO films coated on Si1E17, Si1E17_Au10nm (i.e., Si1E17 coated with 10-nm Au layer), and Si1E17_Au20nm (i.e., Si1E17 coated with 20-nm Au layer). Obviously, these coating films present smooth and homogeneous surface without holes, except for the case of PS film on Si1E17_Au10nm (Figure 5 (C)). Note that the occurrence of hole spots was also observed for the PS film on Si1E0_Au10nm (data not shown). Thus, the 10-nm Au layer was discarded for PS coating; however, it remained in competition for the PS-ZnO coating. The search for the cause of these spots involved

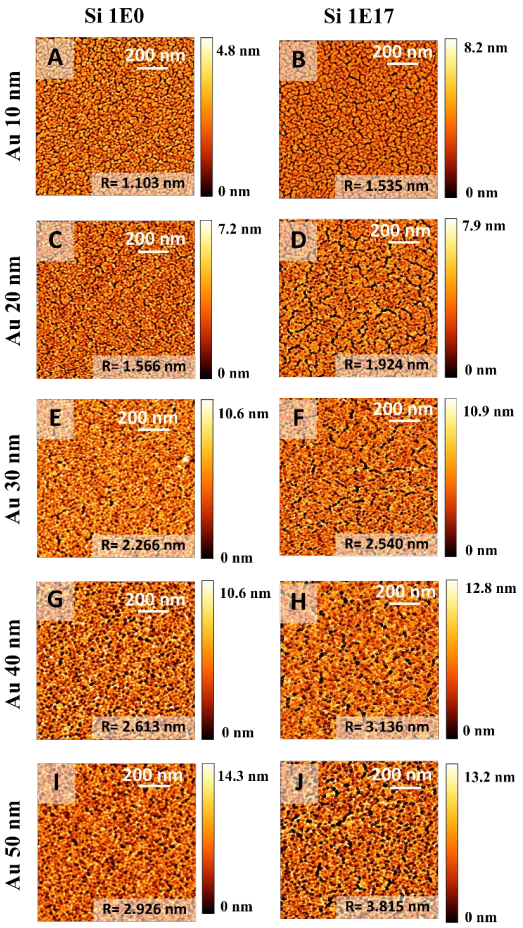


Figure 3. AFM topography images of Au films of different thicknesses on Si1E0 and Si1E17. Parameter *R* at the bottom-right corner of each image represent surface roughness.

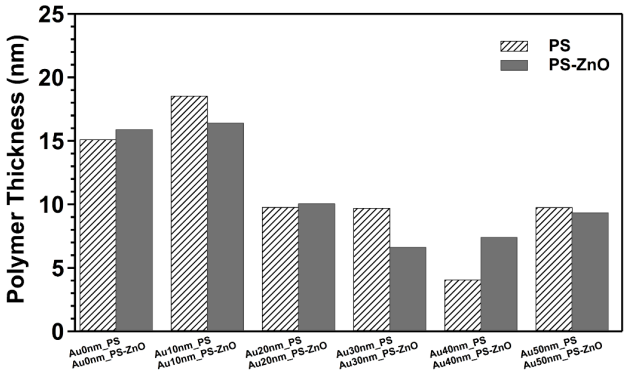


Figure 4. Thickness of the PS and the PS-ZnO films coated on the Au layers on Si. The PS and the PS-ZnO film thicknesses on bare Si are also shown for reference.

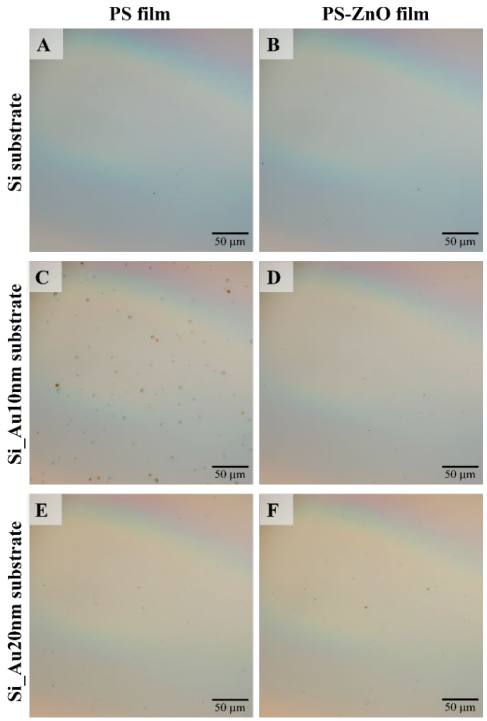


Figure 5. OM images of as-cast PS and PS-ZnO films on Si1E17, Si1E17_Au10nm, and Si1E17_Au20nm substrate (500X magnification)

the use of SEM and EDX. The results are depicted in Figure 6. Based on the acquired data revealing that the chemical compositions of the spot areas (the red-color spectrum in Figure 6 (B)) and the smooth areas of film surface (the blue-color spectrum in Figure 6 (B)) were not significantly different, there were no impurities or other compounds formed during film preparation. As a result, the spot could have been correlated with an interfacial structure formed between the bottom surface of the PS film and the top surface of the 10-nm Au layer.

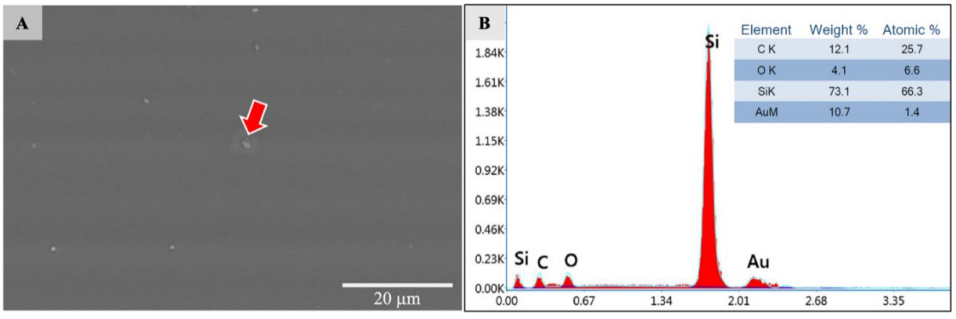


Figure 6. (A) SEM topography image with (B) energy-dispersive X-ray spectroscopy (EDX) analysis of as-cast PS film on Si1E17_Au10nm (5,000X magnification). The red-colored spectrum and the blue-colored spectrum are related to the spot and the smooth areas of film surface.

3.3 Surface energies

Before heating to test the thermal resistance of the coating films and to investigate dewetting inhibition dynamics, the surface energies of the Au layers on Si and the surface energies of PS layers coated on the Au layers were estimated. The necessity is associated with that the annealing temperature and time duration not only reduce the surface energy of polymeric coating film but also decrease the interface energy between the film and the substrate, which induces thermal dewetting [33]. Herein, the wetting analysis was used to calculate surface energy based on both the dispersive components (γ^d) and the polar components (γ^h). At least 3 areas of each sample surface were examined by applying a drop of 0.2 mL of DI-water and a drop of 0.2 mL diiodomethane to each area and then measuring the contact angles between each sample area surface and the droplets. Surface energy was calculated using Owens and Wendt's method, and the constant values of water and diiodomethane surface tensions were utilized. The results are summarized in Table 2 and Figure 7.

Table 2. Calculated surface energies and the related components

Material	θ water (°)	θ diiodomethane (°)	γ^d_{sv} (mJ/m^2)	γ^h_{sv} (mJ/m^2)	γ_s (mJ/m^2)
Si1E0_Au10nm	79.64±2.62	46.39±0.81	35.69	4.42	40.11
Si1E0_Au20nm	81.97±4.09	44.63±2.50	36.62	3.41	40.03
Si1E0_Au10nm_PS30K	89.19±0.44	27.64±0.83	44.46	0.57	45.03
Si1E0_Au20nm_PS30K	88.48±0.58	31.14±1.40	43.05	0.88	43.93
Si1E17_Au10nm	78.11±7.79	40.66±1.02	38.66	4.31	42.97
Si1E17_Au20nm	76.85±4.16	40.48±2.30	38.75	4.75	43.50
Si1E17_Au10nm_PS30K	90.38±0.57	23.80±1.50	45.84	0.40	46.24
Si1E17_Au20nm_PS30K	90.68±1.70	27.45±1.66	44.53	0.45	44.98

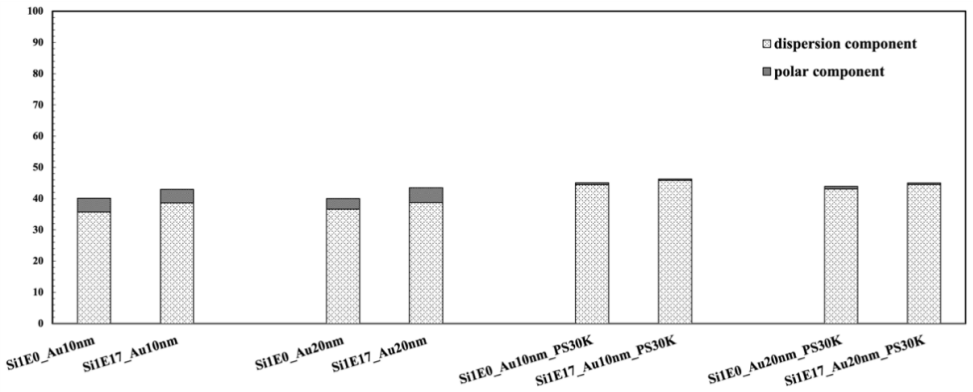


Figure 7. A plot of surface energies of sample surfaces, in which the fractions of contribution from dispersion component and polar component are depicted.

In the case of both 10-nm and 20-nm Au, the Au layer on Si1E0 shows a slight decrease in surface energy compared to the Au layer on Si1E17. The surface energy is ~ 40 mJ/m^2 for Au on Si1E0 while it is ~ 43 mJ/m^2 for Au on Si1E17. Intriguingly, for each Si doping concentration, the rougher Au film surface related to thicker Au film (i.e., 20 nm) possesses approximately the same surface energy as the smoother Au film surface related to the thinner Au film (i.e., 10 nm). Moreover, for each Au thickness, the rougher Au film on Si1E17 provides higher surface energy than the smoother Au film on Si1E0. Such observations suggest that roughness alone cannot describe the variation in surface energy of Au inter-layer and the corresponding thermodynamics of the polymeric coating film [34, 35].

Notably, such variations of surface energy remain the same when coated with PS although the improvement of surface energy is achieved for all the samples (i.e., increasing from ~ 40 mJ/m^2 to ~ 44 mJ/m^2 when coated on Au layers on Si1E0 and from ~ 43 mJ/m^2 to ~ 45 mJ/m^2 when coated on Au layers on Si1E17). However, despite the increased surface energies when coated with PS, the water contact angles on the PS films appear larger while those of the diiodomethane droplet are smaller compared to the angles on Au layers, which can be attributed to the contribution from the increased dispersive component and the decreased polar component. Note that since the fraction of polar component significantly decreases when coated with PS, the influence of Au related to the polar component on the thermal dewetting suppression of polymeric coating films is suggested [14]. It should be noted from our previous study that the addition of ZnO into PS does not change the surface energy of the polymer film, for which the surface energy of PS-ZnO for PS30K was ~ 45 mJ/m^2 [16].

3.4 Dewetting behaviors

After heating at 150^{o}C for 3 h in a vacuum oven chamber, dewetting holes are observed throughout the surface of both PS and PS-ZnO films coated on bare Si substrates (i.e., the reference templates). On Si_Au10nm, while the PS-ZnO coating shows thermal stability, a number of small holes are observed throughout the PS film. However, with the presence of the 20-nm Au interlayer, both coating formulas (i.e., PS and PS-ZnO) produce durable coating films. The increase of the annealing time to 144 h, and the evolution of the coating films are shown in Figure 8, which showed images taken by SEM at the magnification of 10,000X.

It is obvious that the dewetting holes of PS and PS-ZnO films on bare Si substrates are enlarged. While the longer heating time boosts the dewetting of PS film on Si_Au10nm substrate, it also generates dewetting holes in the case of the PS-ZnO film on Si_Au10nm and the PS film on Si_Au20nm. Interestingly, there is still no sign of film rapturing for PS-ZnO on Si_Au20nm. The results indicated that while the addition of ZnO nanofillers can efficiently suppress the thermal dewetting of PS thin films, the Au sheets also contribute to the stability. For instance, regarding the use of PS-ZnO as the coating film to protect transparent Au areas on Si substrate, scaling down the thickness of the Au material to 20 nm not only provides the desired Au properties (i.e., transparency, conductivity, and low consumption of material) but also efficiently enhances the stability of the polymeric coating film. Note that these effects occur for both Si1E0 and Si1E17 substrates.

For quantitative comparison, the calculated percentage of dewetting area of each sample is illustrated in Figure 9. Compared to the dewetting percentages of the PS and PS-ZnO films on bare Si, the effectiveness of 10-nm Au layer to suppress the thermal dewetting is about 10 times for PS coating and about 5 times for PS-ZnO coating. However, the use of 20-nm Au layer can reduce the dewetting percentage by about 14 times for PS coating and to infinity for PS-ZnO coating. The latter is due to the fact that no dewetting occurs for the PS-ZnO coating film when using the 20-nm Au layer.

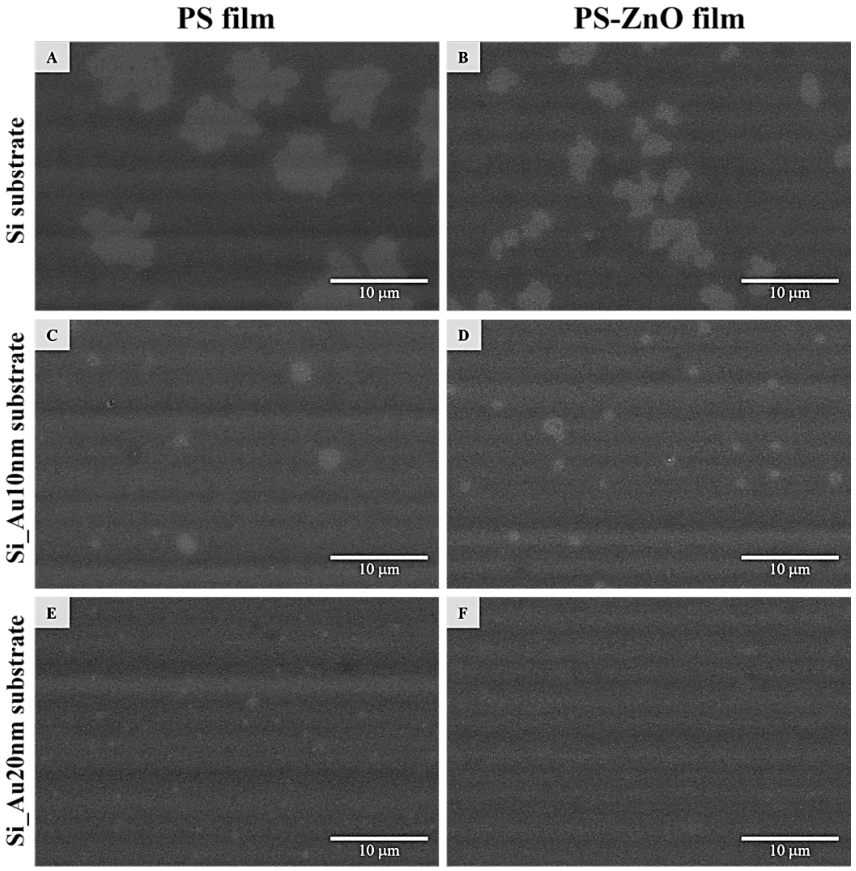


Figure 8. SEM topography images of PS and PS-ZnO thin films on Si1E17, Si1E17_Au10nm, and Si1E17_Au20nm after annealing at 150°C for 144 h (10,000X magnification).

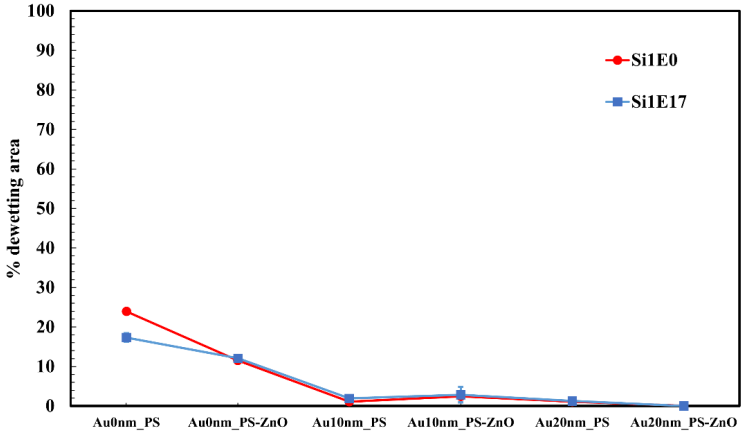


Figure 9. Percentages of dewetting area of PS and PS-ZnO thin films coated on various substrates after annealing at 150°C for 144 h.

To further test the superior dewetting inhibition of the PS-ZnO film on 20-nm Au layer, the samples were heated further at 150°C until 240 h. While the dewetting holes grow in size and number with the heating time for the other coating structures, the PS-ZnO film coated on the Si_Au20nm substrate remains smooth and continuous as shown in Figure 10. Such thermal durability confirms that the dimensional characteristic (i.e., thickness) of the coated Au layer has a significant impact on the stability of the coating polymer film. Considering the use of PS-ZnO to coat transparent Au areas on Si substrate, miniaturizing Au layer thickness to around 20 nm is preferable.

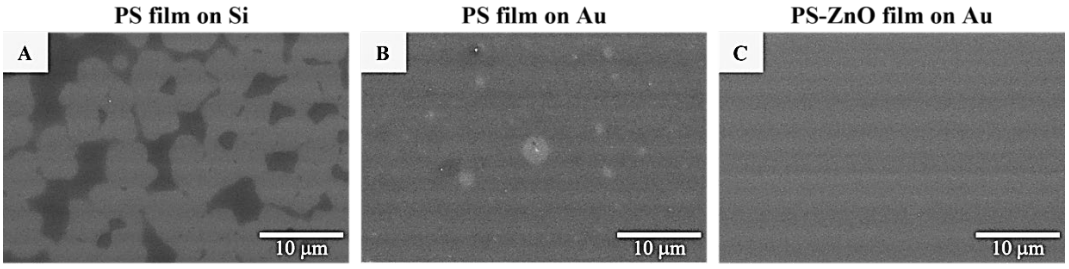


Figure 10. SEM topography images of (A) PS on Si1E0, (B) PS on Si1E0_Au20nm and (C) PS-ZnO on Si1E0_Au20nm after annealing at 150°C for 240 h (10,000X magnification).

The thermal dewetting resistance of the polymeric coating films can be attributed to various factors. Firstly, it can be ascribed to Au film roughness which increases with Au film thickness since the polymer film is more stable when using thicker Au films. However, the increment of roughness due to the increase in Si doing concentration does not likely enhance the coating stability. Accordingly, the parameter describing the dewetting inhibition enhancement does not appear to be the morphological characteristic (i.e., roughness). Other factors such as chemical bonds and polar forces associated with the dominant (111) orientation of Au film can also contribute. Electronically, considering that the 20-nm Au film possesses higher content of Au than the 10-nm Au film, a higher density of free electrons can be expected along the Au surface. The intensified surface potential probably more strongly attracts the positive polar points in the polymer matrix. Notably, since the coating stability does not improve with Si doping concentration, the internal electric potential due to band bending in the Si layer is unlikely to contribute to polymer chain dynamics. Assuming that all influences from the coated Au layer are identical for the examined Au thicknesses, the thickness of the polymer film can also be a crucial parameter due to the length of the interfacial interactions.

4. Conclusions

This work reported the examination of thermal stability of PS films and PS-ZnO films coated on Au nano-layer with different thicknesses on Si substrate to determine the smallest Au film thickness at which the polymeric coating films exhibited the optimal resistance to thermal dewetting. The effect of the Au component on the inhibition of thermal dewetting was also discussed. On the basis that requires transparent and conductive Au electrode, 20-nm Au film was identified as the optimal Au layer on which both PS and PS-ZnO films were stable at the environment temperature of 150°C for up to 3 h. However, it was the PS-ZnO film that showed outstanding thermal stability for up to 240 h. Such excellent durability was attributed to the physical-chemical concept that the coating film

could experience various forces from the coated layers that affected the mobility of polymer chains. Considering the increase of Au content and Au film roughness with increasing Au film thickness together with the realization of their similar surface adhesion forces, the possible influential parameters of Au material on the stability of PS matrix were discussed. The findings not only provide insight into heat-resistant coating for Au layers grown on Si but can also be of benefit in the design and understanding of relevant electronic protection and functional polymeric coating. More specifically, the research findings should be of benefit in the miniaturization of devices to improve performance as well as the concurrent scaling-down of coating films.

5. Acknowledgements

This research was funded by the Faculty of Applied Science, King Mongkut's University of Technology North Bangkok (KMUTNB) with Contract Number 652120 and also by the National Science Research and Innovation Fund (NSRF) with Contract Number KMUTNB–FF–65–57. The growth of Au nano-thin layers using the sputtering technique and characterizing using the AFM and TEM techniques were sponsored by the National Nanotechnology Center (NANOTEC), National Science and Technology Development Agency (NSTDA). This work was also sponsored by the Scientific Instrument and High-Performance Computing Center (SICC) at KMUTNB for SEM characterization.

References

[1] Mihelčič, M., Klanjšek, G.M. and Slemenik, P.L., 2022. Rheological behavior of spectrally selective coatings for polymeric solar absorbers. *Coatings*, 12(3), DOI: 10.3390/coatings12030388.

[2] Cai, X.J., Yuan, H.M., Blencowe, A., Qiao, G.G., Genzer, J. and Spontak, R.J., 2015. Film-stabilizing attributes of polymeric core-shell nanoparticles. *ASC Nano*, 9(8), 7940-7949. DOI: 10.1021/acsnano.5b00237.

[3] Bal, J.K., Beuvier, T., Unni, A.B., Panduro, E.A.C., Vignaud, G., Delorme, N., Chebil. M.S., Grohens, Y. and Gibaud, A., 2015. Stability of polymer ultrathin films (<7 nm) made by a top-down approach. *ASC Nano*, 9(8), 8184-8193, DOI: 10.1021/acsnano.5b02381.

[4] Barkley, D.A., Jiang, N., Sen, M., Endoh, M.K., Ruidick, J.G., Koga, T., Zhang, Y., Gang, O., Yuan, G., Satija, S.K., Kawaguchi, D., Tanaka, K. and Karim, A., 2017. Chain conformation near the buried interface in nanoparticle-stabilized polymer thin films. *Macromolecules*, 50(19), 7657-7665, DOI: 10.1021/acs.macromol.7b01187.

[5] Lee, S., Lee, W., Yamada, N.L., Tanaka, K., Kim, J.H., Lee, H. and Ryu, D.Y., 2019. Instability of polystyrene film and thermal behaviors mediated by unfavorable silicon oxide interlayer. *Macromolecules*, 52(19), 7524-7530, DOI: 10.1021/acs.macromol.9b01284.

[6] Pahlavanm, A.A., Cueto-Felgueroso, L., Hosoi, A.E., McKinley, G.H. and Juanes, R., 2018. Thin films in partial wetting: stability, dewetting and coarsening. *Journal of Fluid Mechanics*, 845, 642-681, DOI: 10.1017/jfm.2018.255.

[7] Baglioni, M., Montis, C., Brandi, F., Guaragnone, T., Meazzini, I., Baglioni, P. and Berti, D., 2017. Dewetting acrylic polymer films with water/propylene carbonate/surfactant Mixtures – Implications for cultural heritage conservation. *Physical Chemistry Chemical Physics*, 19(35), 23723-23732, DOI: 10.1039/c7cp02608k.

[8] Kubo, M., Takahashi, Y., Fuiji, T., Liu, Y., Sugioka, K.I., Tsukada, T., Minami, K. and Adschiri, T., 2014. Thermal dewetting behavior of polystyrene composite thin films with organic-modified inorganic nanoparticles. *Langmuir*, 30(29), 8956-8964, DOI: 10.1021/la502009x.

[9] Pangpaiboon, N., Traiphol, N., Promarak, V. and Traiphol, R., 2013, Retradation the dewetting dynamics of ultrathin polystyrene films using highly branched aromatic molecules as additives. *Thin Solid Films*, 548, 323-330, DOI: 10.1016/j.tsf.2013.09.059.

[10] Pangpaiboon, N., Traiphol, N. and Traiphol, R., 2015. Enhancing the stability of polystyrene ultrathin films by using star-shape polymers as dewetting inhibitors. *Journal of Coating Technology and Research*, 12, 1173-1183, DOI: 10.1007/s11998-015-9715-y.

[11] Liu, Y., Kato, T., Kubo, M., Sugioka, K. I., Tsukada, T., Takami, S. and Adschiri, T., 2015. Annealing-promoted unidirectional migration of organic-modified nanoparticles embedded two-dimensionally in polymer thin films. *Journal of Applied Polymer Science*, 132, DOI: 10.1002/app.42760.

[12] Roy, S., Bandyopadhyay, D., Karim, A. and Mukherjee, R., 2015. Interplay of substrate surface energy and nanoparticle concentration in suppressing polymer thin film dewetting. *Macromolecules*, 48(2), 373-382, DOI: 10.1021/ma501262x.

[13] Pangpaiboon, N. and Traiphol, N., 2014. Dewetting suppression of polystyrene thin films using titanium dioxide nanoparticles. *Key Engineering Materials*, 608, 218-223, DOI: 10.4028/www.scientific.net/kem.608.218.

[14] Thapoung, J., Tasurin, K., Traiphol, N. and Pangpaiboon, N., 2018. The effects of concentrations of ZnO nanoparticles on dewetting suppression of PS thin films. *Journal of Metal, Materials and Minerals*, 28(2), 89-93.

[15] Tumsarp, P., Pangpaiboon, N., Sujaroon, K., Deejai, S., Treetong, A., Sae-Ueng, U. and Sinthiptharakoon, K., 2020. Inorganic nanoparticle-blended polymer nanofilm and its wettability improvement: Film grading and dewetting cause analysis. *Applied Surface Science*, 521, DOI: 10.1016/j.apsusc.2020.146399.

[16] Sujaroon, K., Whangdee, P. and Pangpaiboon, N., 2020. Effect of polystyrene molecular weight and zinc oxide concentration on dewetting behavior of polymeric thin films. *Journal of Metals, Materials and Minerals*, 30(2), 58-66, DOI: 10.14456/jmmm.2020.21.

[17] Hongfang, W., Drew, E., Nicolas, V., Hans, G. and Laurence, M., 2019. Interfacial forces at layered surfaces: substrate electrical double layer forces acting through ultrathin polymer coatings. *Langmuir*, 35, 11679-11689, DOI: 10.1021/acs.langmuir.9b02176.

[18] Li, B., Chen, L., Zhang, S., Tao, Q., Ma, Y.H., Hu, P., Lu, X., Chou, K.C. and Chen, Z., 2023. Absolute molecular structure of the polystyrene at the buried polystyrene/silica interface and its relationship to dewetting during annealing. *Applied Surface Science*, 611(A), DOI: 10.1016/j.apsusc.2022.155715.

[19] Amarandei, G., O' Dwyer, C., Arshak, A. and Corcoran, D., 2013. The stability of thin polymer films as controlled by changes in uniformly sputtered gold. *Soft Matter*, 9(9), 2695-2702, DOI: 10.1039/c3sm27130g.

[20] Piedade, A.P., Romeu, F., Branco, R. and Morais, P.V., 2018. Thin films for medical and environmental applications. In: L. Nánai, A. Samantara, L. Fábián and S. Ratha, eds. *Methods for Film Synthesis and Coating Procedures*. Croatia: IntechOpen, pp. 1-13.

[21] Kaune, G., Ruderer, M.A., Metwalli, E., Wang, W., Couet, S., Schlage, K., Röhlsberger, R., Roth, S.V. and Müller-Buschbaum, P., 2009. In situ GISAXS study of gold film growth on conducting polymer films. *ACS Applied Materials and Interfaces*, 1(2), 353-360, DOI: 10.1021/am8000727. PMID: 20353223.

[22] Shankar, S. and Rhim, J.W., 2019. Effect of types of zinc oxide nanoparticles on structural, mechanical and antibacterial properties of poly(lactide)/poly(butylene adipate-co-terephthalate) composite films. *Food Packaging and Shelf Life*, 21, DOI: 10.1016/j.fpsl.2019.100327.

[23] Rojas, K., Canales, D., Amigo, N., Montoille, L., Cament, A., Rivas, L.M., Castell, O.G., Reyes, P., Ulloa, M.T., Greus, A.R. and Zapata, P.A., 2019. Effective antimicrobial materials based on low-density polyethylene (LDPE) with zinc oxide (ZnO) nanoparticles. *Composites Part B*, 172, 173-178, DOI: 10.1016/j.compositesb.2019.05.054.

[24] Jayakumar, A., Heera, K.V., Sumi, T.S., Joseph, M., Mathew, S., Praveen, G., Nair, I.C. and Radhakrishnan, E.K., 2019. Starch-PVA composite films with zinc-oxide nanoparticles and phytochemicals as intelligent pH sensing wraps for food packaging application. *International Journal of Biological Macromolecules*, 136, 395-403, DOI: 10.1016/j.ijbiomac.2019.06.018.

[25] Sinthiptharakoon, K., Sapcharoenkun, C., Nuntawong, N., Duong, B., Wutikhun, T., Treetong, A., Meemuk, B., Kasamechonchung, P. and Klamchuen, A., 2018. Conductive scanning probe microscopy of the semicontinuous gold film and its SERS enhancement toward two-step photo-induced charge transfer and effect of the supportive layer. *Applied Surface Science*, 441, 364-371, DOI: 10.1016/j.apsusc.2018.01.269.

[26] Wu, X., Dai, D., Ling, Y., Chen, S., Huang, C., Feng, S. and Huang, W., 2020. Organic single-crystal transistor with unique photo responses and its application as light-simulated synaptic devices. *ACS Applied Materials and Interfaces*, 12(27), 30627-30634, DOI: 10.1021/acsami.0c05809.

[27] Baptista, A., Silva, F., Porteiro, J., Míguez, J. and Pinto, G., 2018. Sputtering physical vapour deposition (PVD) coatings: a critical review on process improvement and market trend demands. *Coatings*, 8(11), DOI: 10.3390/coatings8110402.

[28] Huang, S.Y., Hsieh, P.Y., Chung, C.J., Chou, C.M. and He, J.L. 2022. Nanoarchitectonics for ultrathin gold films deposited on collagen fabric by high-power impulse magnetron sputtering. *Nanomaterials*, 12(10), DOI: 10.3390/nano12101627.

[29] Erbil, H.Y., 2006. *Surface Chemistry of Solid and Liquid Interface.* Oxford: Blackwell Publishing Ltd.

[30] Kapranos, P., Carney, C., Pola, A. and Jolly, M., 2014. Advanced casting methodologies: investment casting, centrifugal casting, squeeze casting, metal spinning, and batch casting. In: S. Hashmi, ed. *Comprehensive Materials Processing. Vol. 5.* Amsterdam: Elsevier, pp. 39-67.

[31] Tatarkin, D.E., Yakubovsky, D.I., Ermolaev, G.A., Stebunov, Y.V., Voronov, A.A., Arsenin, A.V., Volkov, V.S. and Novikov, S.M., 2020. Surface-Enhanced Raman spectroscopy on hybrid graphene/gold substrates near the percolation threshold. *Nanomaterials*, 10(1), DOI: 10.3390/nano10010164.

[32] Liu, X., Han, Y., Evans, J.W., Engstfeld, A.K., Behm, R.J., Tringides, M.C., Hupalo, M., Lin, H., Huang, L., Ho, K., Appy, D., Thiel, P.A. and Wang, C., 2015. Growth morphology and properties of metals on graphene. *Progress in Surface Science*, 90(4), 397-443, DOI: 10.1016/j.progsurf.2015.07.001.

[33] Quan, J., Zhang, J., Qi, X., Li, J., Wang, N. and Zhu, Y., 2017. A study on the correlation between the dewetting temperature of Ag film and SERS intensity. *Scientific Reports*, 7(1), DOI: 10.1038/s41598-017-15372-y.

[34] Kazzi, Y., Awada, H. and Nardin, M., 2010. Adhesion on nanoorganized multilayers: surface thermodynamics and local energy dissipation. *Advances in Physical Chemistry*, 2010, DOI: 10.1155/2010/502709.

[35] Atay, N.O., Osman, B., Akgol, S., Karagozler, A. and Denizli, A., 2018. Preparation of molecularly imprinted SPR nanosensor for myoglobin detection. *Current Applied Polymer Science*, 2(2), 102-111, DOI: 10.2174/2452271602666180828103017.